


Numerical simulation of virus-laden droplets transport from lung to lung by using eighth-generation airway model

Shohei Kishi¹, Masashi Yamakawa¹^[0000-0001-5960-2602], Ayato Takii²^[0000-0003-3257-7640],
Tomoaki Watamura¹^[0000-0002-4217-7109], Shinichi Asao³^[0000-0003-4326-8480], Seiichi
Takeuchi³, Minsuok Kim⁴^[0000-0003-1074-8082]

¹ Kyoto Institute of Technology, Matsugasaki, Sakyo-ku, Kyoto 606-8585, Japan

² RIKEN Center for Computational Science, 7-1-26 Minatojima-minami-machi, Chuo-ku,
Kobe, Hyogo 650-0047, Japan

³ College of Industrial Technology, 1-27-1 Amagasaki, Hyogo, 661-0047, Japan

⁴ School of Mechanical, Electrical and Manufacturing Engineering, Loughborough University,
Loughborough, UK
m2623010@edu.kit.ac.jp

Abstract. In this study, we simulated the trajectory of virus-laden droplets from the lung of an infected person to that of the exposed person using computational fluid dynamics. As numerical models, the model of the infected person who had a bifurcated airway and that of the exposed person who had an eighth-generation airway were prepared. The volume and number of virus-laden droplets adhered to the inlet patches of the exposed person's lung were calculated to evaluate the risk of infection when the infected person was talking for 40 seconds. To identify the lung to which droplets adhered, we labeled the inlet patches of the exposed person's lung with 53 numbers, and then measured the volume and number of droplets on the inlet patches of lung. We also categorized the lung's 53 intake patches into five groups and calculated the overall volume and number of attached droplets for each. In addition, we parameterized the angle of the exposed person's neck to evaluate the effect of the tilting neck on the volume and number of droplets reaching the lungs. We found that the volume and number of droplets adhered to the right middle group of bronchi were remarkably smaller than the other four groups, and weakly depended on the neck angle. The volume and number of droplets adhered to the inlet patches of the lung reached the maximum values when the neck angle was 20° upward.

Keywords: Computational fluid dynamics, Respiratory organ, SARS-CoV-2.

1 Introduction

Quantitative and effective methods of preventing infection are still required owing to the ongoing spread of SARS-CoV-2. Since respiratory viruses such as SARS-CoV-2 and influenza are mainly transported through the air [1], it is necessary to determine how the exposed person takes in virus-laden droplets, i.e., the route of airborne

transportation. There are two major methods for identifying the routes of airborne infection: the first is an experimental method using actual rooms and subjects, and the second is a simulation method using numerical calculations. As a typical example of experimental methods, Killingley et al. [2] performed SARS-CoV-2 human investigation in 2022. They intranasally inoculated human with SARS-CoV-2, and identified the dose of virus causing infection and evaluated the symptom kinetics during infection. These experimental approaches offer the advantage of collecting precise and reliable data, whereas they have the drawback of requiring a great deal of time and manpower.

On the other hand, computer simulations can efficiently reproduce this phenomenon. Actually, computational fluid dynamics (CFD) has been actively used in recent years [3-5]. Ramajo et al. [3] simulated how an urban bus's HVAC (Heat, Ventilation, Air Conditioning) system would affect the movement of virus-laden droplets. It was found that the large droplets ($>200\mu\text{m}$) were not captured by HVAC outlet; they moved more than 3m and deposited within 2 seconds. Small droplets ($<5\mu\text{m}$) were more sensitive to the airflow and were easily trapped by HVAC. Mariam et al. [4] also simulated the dispersion of SARS-CoV-2 in an indoor environment. They parameterized the location of the air vent and the velocity of expelled particles. They found that the airflow, during normal talking, transports virus-laden droplets from the particle generator to receptor, when there is 2m distance between them. As an example of studies focusing on the airway, Wedel et al. [5] adopted three different airway models to simulate variation in the aerosol deposition during breathing. They reported that the deposition variation in the laryngeal region depended on the shape of the airway.

Although there are numerous studies examining the interior and exterior of the human body separately, no study has examined both regions together. In addition, while many studies have parameterized the velocity of particle generation and the position of air vent as variables, there are few cases where the angle of neck is parameterized [6]. It can be thought that tilting neck alters the shape of flow pathway in the airway. Doing so, it is expected the transportation route of virus-laden droplets will be changed, which makes the differences in the volume and number of droplets adhered to the lung. Investigating this difference, we hypothesized the change of neck angle may lead to some degree of reducing the risk of infection. In this study, we parameterized the angle of the exposed person's neck and comprehensively analyzed the human body's internal and external flow fields. The movement of droplets was also calculated using the fluid analysis results to simulate how many virus-laden droplets expelled from the infected person's lung would adhere the exposed person's lung.

2 Numerical approach

2.1 Flow field and heat analysis

The flow and temperature fields were calculated employing *SCRYU/Tetra* [7]. The governing equations are the continuity equations, the incompressible Navier-Stokes equations, and the energy conservation equation.

The continuity equation is given by

$$\frac{\partial u_{a_i}}{\partial x_i} = 0. \quad (1)$$

the three-dimensional incompressible Navier-Stokes equations are defined by

$$\frac{\partial(\rho_a u_{a_i})}{\partial t} + \frac{\partial(u_{a_j} \rho_a u_{a_i})}{\partial x_j} = -\frac{\partial p}{\partial x_i} + \frac{\partial}{\partial x_j} \left\{ \mu \left(\frac{\partial u_{a_i}}{\partial x_j} + \frac{\partial u_{a_j}}{\partial x_i} \right) \right\} - \rho_a g_i \beta (T_a - T_0), \quad (2)$$

where u_{a_i} ($i, j = 1, 2, 3$) is the air velocity components in the x , y and z direction, and ρ_a is gas density, which is constant. t , p and μ denote time, pressure, viscosity, respectively. g_i ($i, j = 1, 2, 3$) is the gravity acceleration in the x , y and z direction, and β indicates the thermal expansion coefficient. T_a and T_0 are the air temperature and reference temperature, respectively. The energy conservation equation is given by

$$\frac{\partial(\rho_a C_p T_a)}{\partial t} + \frac{\partial(u_{a_j} \rho_a C_p T_a)}{\partial x_j} = \frac{\partial}{\partial x_j} \left(K \frac{\partial T_a}{\partial x_j} \right) + \dot{q}, \quad (3)$$

where C_p is specific heat capacity. K and \dot{q} denote thermal conductivity and heat flux. The SIMPLeC algorithm [8] was used to solve Eqs. (1) and (2), which couples of velocity and pressure. The second order MUSCL method [9] was applied to the convective terms of Eqs. (2) and (3). The Smagorinsky sub-grid scale (SGS) model of large eddy simulation (LES) [10] is used to accuracy capture eddies generated by turbulence.

2.2 Movement of virus-laden droplets

The equation of droplet radius changing due to evaporation is defined as follows [11]:

$$\frac{dr}{dt} = - \left(1 - \frac{RH}{100} \right) \cdot \frac{D e_s(T_a)}{\rho_d R_v T_a} \cdot \frac{1}{r}, \quad (4)$$

where r is droplet radius, and RH represents humidity. D , e_s and ρ_d denote the water vapor coefficient, saturated vapor pressure, and droplet density, respectively. R_v indicates the gas constant of water vapor. The equation of droplet motion is defined as [11]

$$\frac{4}{3} \pi \rho_d r^3 \frac{dv_i}{dt} = \frac{4}{3} \pi \rho_d r^3 g_i + C_D(v_i) \cdot \frac{1}{2} \rho_a S |u_{a_i} - v_i| (u_{a_i} - v_i), \quad (5)$$

where v_i ($i = 1, 2, 3$) is the droplet velocity components in the x , y and z direction, and C_D denotes the drag coefficient. S is the projected area of droplets.

3 Simulation of droplets

3.1 Numerical model

Figure 1(a) shows the overview of two people facing each other in the room. The room size was $3.0\text{m} \times 3.0\text{m} \times 3.0\text{m}$, and $0.15\text{m} \times 0.15\text{m}$ air vent is placed at the top of the room. The distance between the mouths of two people was set at 1.0m . Figure 1(b) indicates human models with airways for infected and exposed individuals, respectively. In this study, we made a simulation model: the talking infected person and the breathing exposed person.

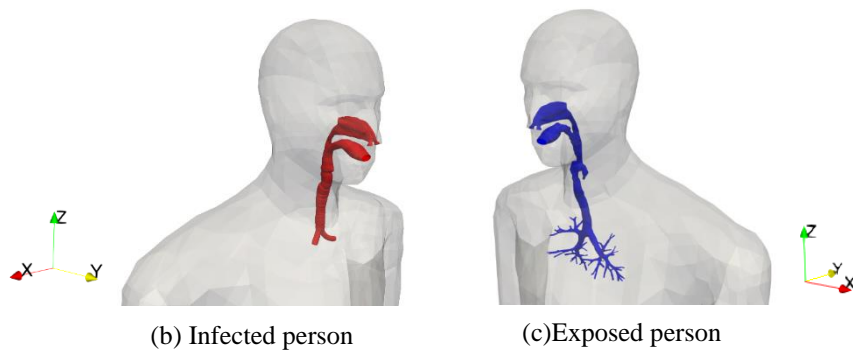
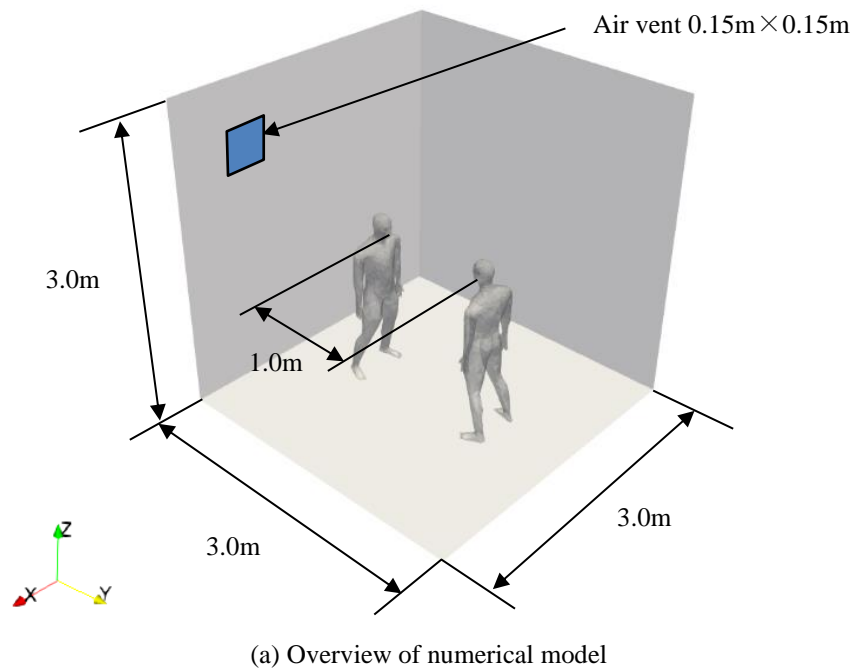


Fig. 1. Numerical model of the room and human model with the airway.

The airway of the infected person is bifurcated and its shape is created based on *Anatomy & Physiology* [12]. The airway of the exposed person is eighth-generation and is modeled from computed tomography (CT) data of adult male [13,14]. Figure 2 shows the tilting motion of exposed person's neck. The rotation axis is placed at the neck center, and the rotation is made upward ranging $\theta = 0$ to 20° with 5° increments. The shape of the airway below the throat is independent of rotation. Figure 3 shows the computational grids of eighth-generation airway model. Computational grids were created by using *SCRYU/Tetra*. The wall of the airway has three prismatic layers. The total number of computational grids inside and outside the human body was approximately 4,000,000. As a typical example, the number of tetrahedron elements is 2,423,944, pyramid elements is 2,208 and prism elements is 1,496,250 in $\theta = 0^\circ$.

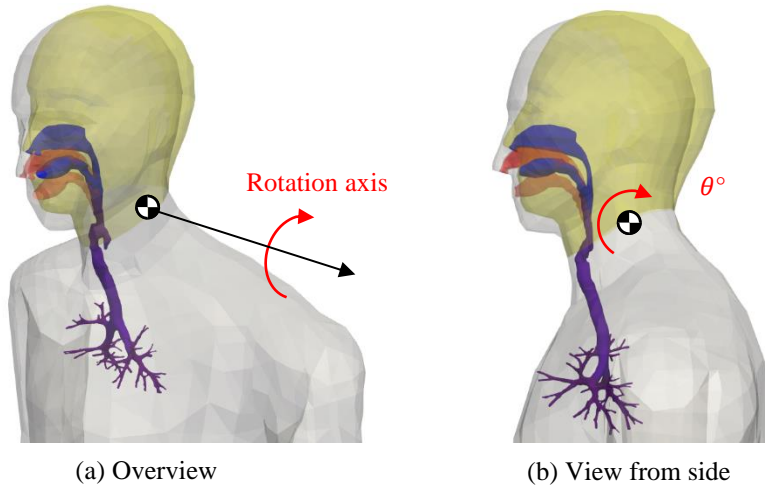


Fig. 2. The angle of neck variation (yellow represents $\theta = 20^\circ$).



Fig. 3. Grids of eighth-generation airway.

3.2 Computational condition for droplets analysis

Figure 4 indicates the frequency distribution of virus-laden droplet diameters expelled from an infected person during talking [15,16]. Although droplets were expelled at 160 pieces/s in the literature, we released droplets at 1,600 pieces/s to achieve better accuracy. The computational time was set to 40 seconds by considering both the time and efficiency required to capture the trend of the phenomenon. The total number of droplets was 64,000. Figure 5 shows the initial position of generating droplets in the infected person's bronchi, which are installed equally on both sides of the airway.

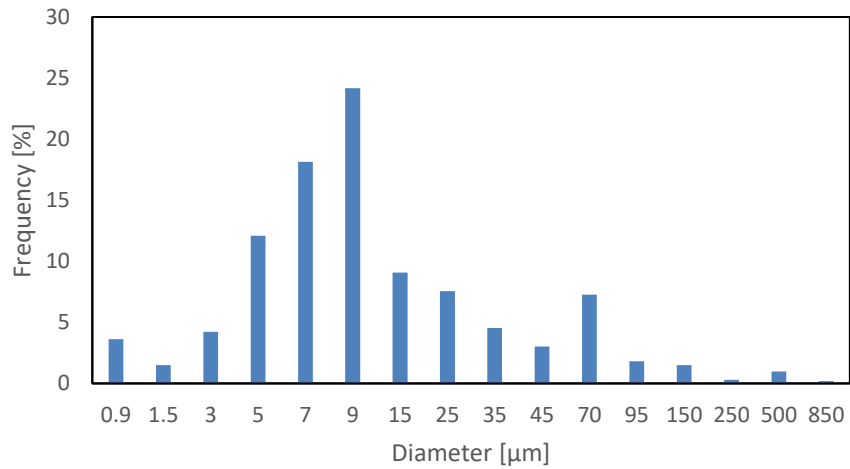


Fig. 4. Frequency distribution of virus-laden droplet diameters expelled from infected person during talking.

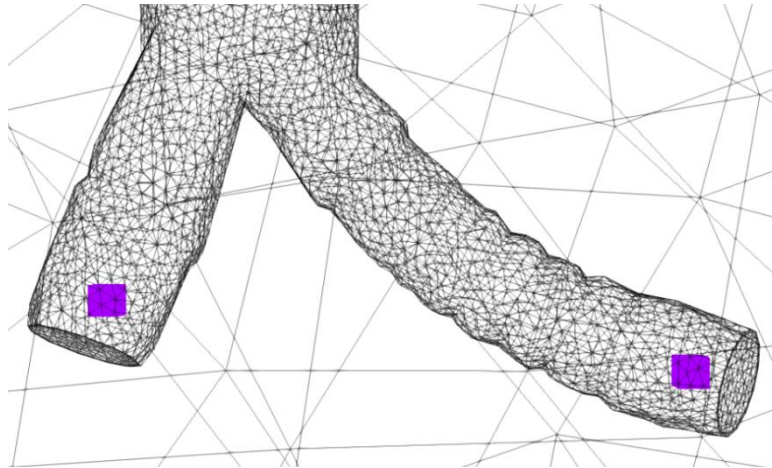


Fig. 5. Initial position of generating droplets (the acral part of infected person's bronchi).

3.3 Assessing the risk of infection

Figure 6(a) shows the overview of the infected person's airway and the inlet patches of the lung, and Fig. 6(b) shows the airway of the exposed person. Note that we defined the lower left bronchi in the human body as Type A and the lower right bronchi as Type B. Figures. 6(c) and 6(d) display the numbers assigned to inlet patches of lung in Type A and Type B, respectively. We followed the method of grouping [17,18]; we grouped the inlet patches of lung No. 1 to 11 as upper left of bronchi (LeftUp), No. 12 to 23 as lower left of bronchi (LeftLow), No. 24 to 34 as upper right of bronchi (RightUp), No. 35 to 38 as middle right of bronchi (RightMid) and No. 39 to 53 as lower right of bronchi (RightLow). In this study, 53 inlet patches of lungs were divided into five groups and the total volume and number of droplets adhered to each group were calculated to facilitate comparison with the literature. The greater the amount of droplets adhered to inlet patches of lungs, the higher the risk of infection is assessed in this study.

3.4 Computational conditions for flow and heat analysis

Figure 7 shows the volume flow rate during talking which was determined from Bale et al. [16] and Gupta et al. [19], and was given at the inlet surfaces of the infection person's lung in Fig. 6(a). Figure 8 shows the volume flow rate of breathing as defined by the Handbook of Physiology [20] and Ogura et al. [21], and was applied at the inlet patches of the exposed person's lung in Figs. 6(c) and 6(d). As pressure condition, the homogeneous Neumann condition was also adopted to the inlet surfaces of both lungs. The air vent in Fig. 1(a) is subjected to the boundary conditions: static pressure is 0 and velocity is the homogeneous Neumann condition. The initial room temperature is $T_r = 20^\circ\text{C}$, and the body temperature of infected and exposed person is $T_h = 30^\circ\text{C}$, considering the effect of clothes. The temperature of air expelled from the infected and the exposed person is assumed to be $T_f = 36^\circ\text{C}$.

Table 1. Computational conditions for calculation flow field and movement of droplets.

Total number of computational grids	About 400,0000
The air vent of room	Velocity: Neumann Pressure: 0
Infected person's lung inlet surface	Velocity: Talking Pressure: Neumann
Exposed person's lung inlet surface	Velocity: Breathing Pressure: Neumann
Initial room temperature	20°C
Human body temperature	30°C
Intake and exhaled air temperature	36°C
Time step of flow calculation	0.0001
Time step of droplets calculation	0.00001

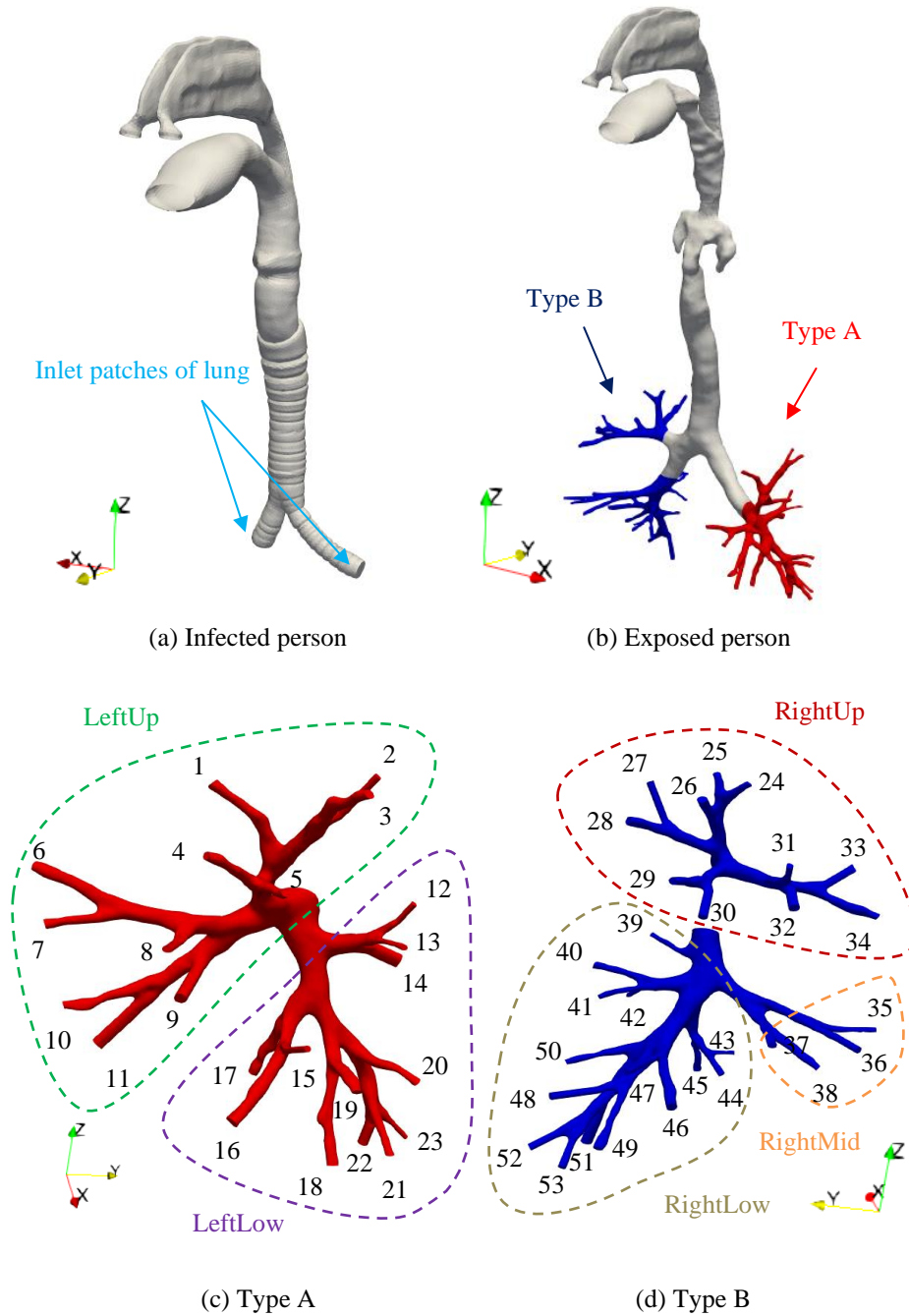


Fig. 6. Enlarged view of the airway.

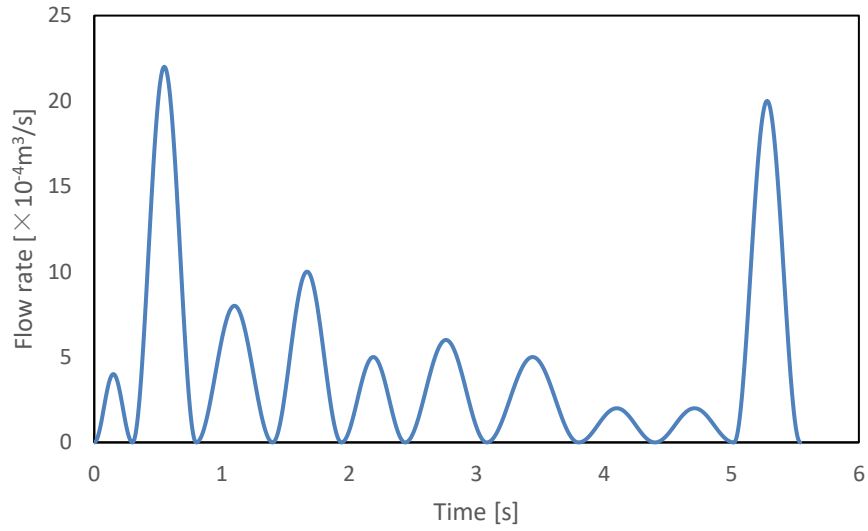


Fig. 7. The volume flow rate during talking.

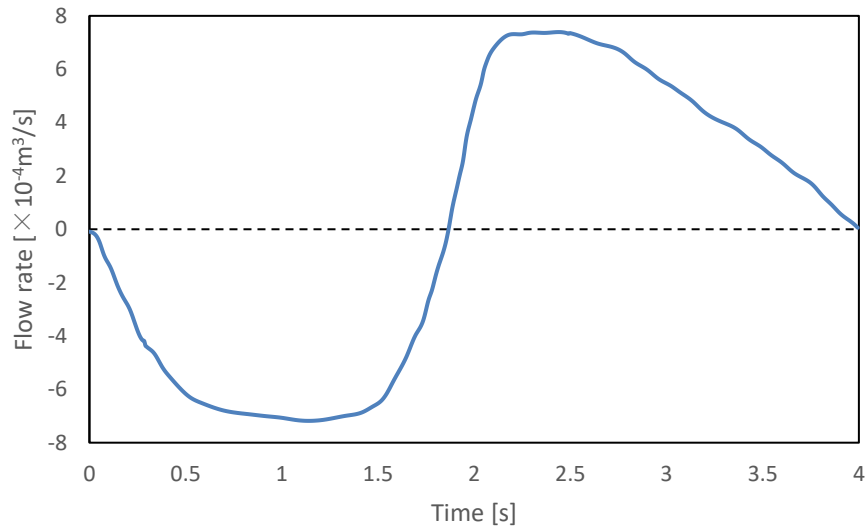


Fig. 8. The volume flow rate of breathing.

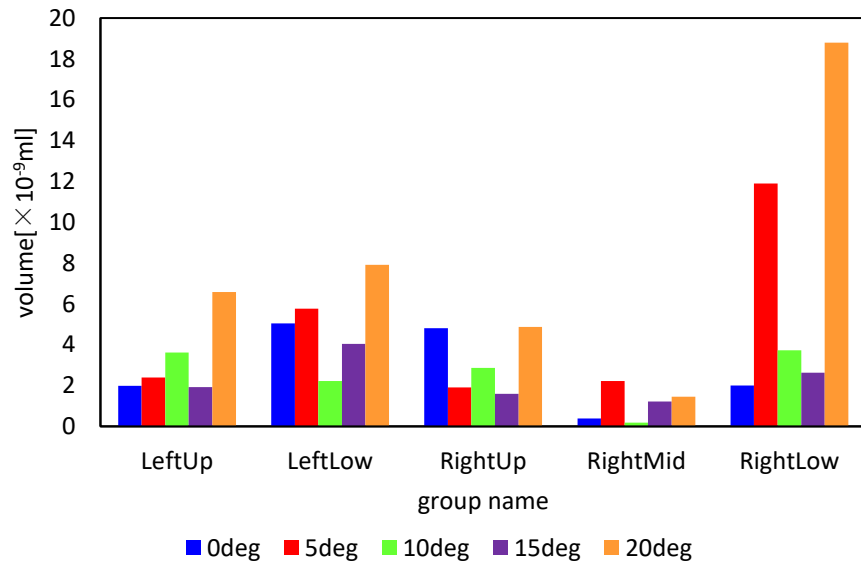
4 Results and discussion of droplets analysis

Figures 9(a) and (b) represent the total volume and number of virus-laden droplets adhered to each of the five groups. The maximum volume is found at RightLow for θ of 5° , 10° , and 20° , while it takes the maximum value at LeftLow in case of $\theta = 0^\circ$ and 15° . The number of adhered droplets is high at RightLow ($\theta = 0^\circ$ and 20°), while it takes the maximum value at LeftLow ($\theta = 5^\circ$, 10° , and 15°). The number of droplets adhered to RightLow ($\theta = 15^\circ$) in Fig. 9(b) is only nine, whereas Fig. 9(a) shows the maximum volume of adhered droplets, and this suggests that the adhered droplets have large volume. Thus, there is a difference between the locations of maximum volume and those of maximum number. As an overall trend, the volume and number of adhered droplets in the RightMid group are smaller than those in the other four groups in Fig. 9. A similar trend was also found in the literature [17], and this is because the number of inlet patches originally grouped together is only four. It was also found that the volume and number of adhered droplets also took large values for each group at $\theta = 20^\circ$. We thought that this finding was due to the difference in airflow pathways generated by tilting neck.

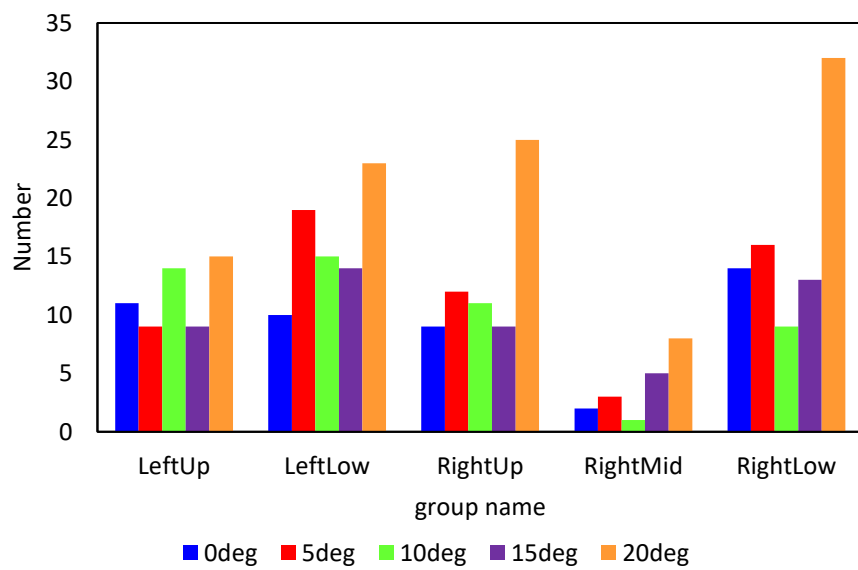
Figure 10 shows the dispersion of virus-laden droplets when θ is 20° . Red and green particles depict floating droplets and adhered droplets, respectively. The human model on the left side is the infected person releasing virus-laden droplets while the model on right is the exposed person who inhales the droplets by breathing. The droplets are released slightly downward because the oral cavity of infected person is curved, as shown in Fig. 6(a). Therefore, it can be seen that many droplets adhere to the torso of the exposed person. It is also confirmed that many droplets are floating over the head of the exposed person. We thought that the updrafts generated by the heat of the exposed person caused droplets to float.

Figure 11 indicates the streamline of the exposed person when the volume flow rate of inhalation took the maximum value. It can be seen that the airflow from mouth to lungs is fast at the throat with a speed of approximately 4 m/s. The exposed person in Fig. 11(b) is more likely to inhale the air located at a higher place because the mouth of exposed person is facing upward. This finding suggests that tilting the neck upward facilitates the aspiration of droplets raised by updrafts. It was also confirmed that the shape of the flow pathway in the airway of Fig. 11(a) is curved entirely, while that of Fig. 11(b) is straight from the throat to the lungs. This could be explained by tilting the neck upward, which allowed droplets inhaled into the oral cavity to fall into the lungs.

From the above description, it was concluded that tilting the neck upward led to change of airflow pathways in respiratory and room regions, which increased the number of droplets inhaled by the exposed person, and the volume and number of droplets adhered to the inlet patches of lungs took considerable value. Therefore, keeping the head forward could suppress the inhalation of droplets raised by the updrafts, and reduce the risk of infection.



(a) Volume



(b) The number of droplets

Fig. 9. The volume and the number distribution of virus-laden droplets per bronchial group.

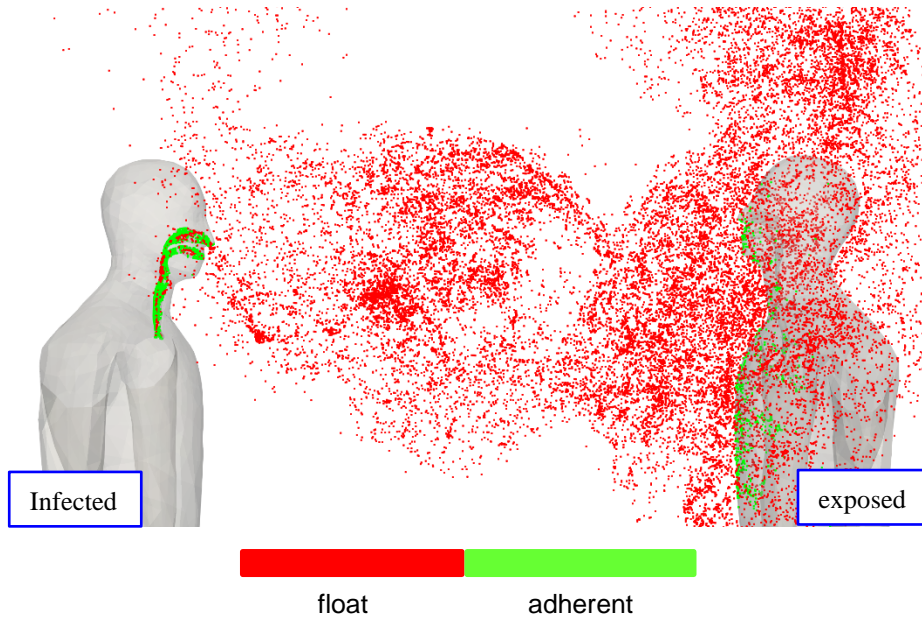


Fig. 10. Dispersion of virus-laden droplets ($\theta = 20^\circ$, $t = 40s$).

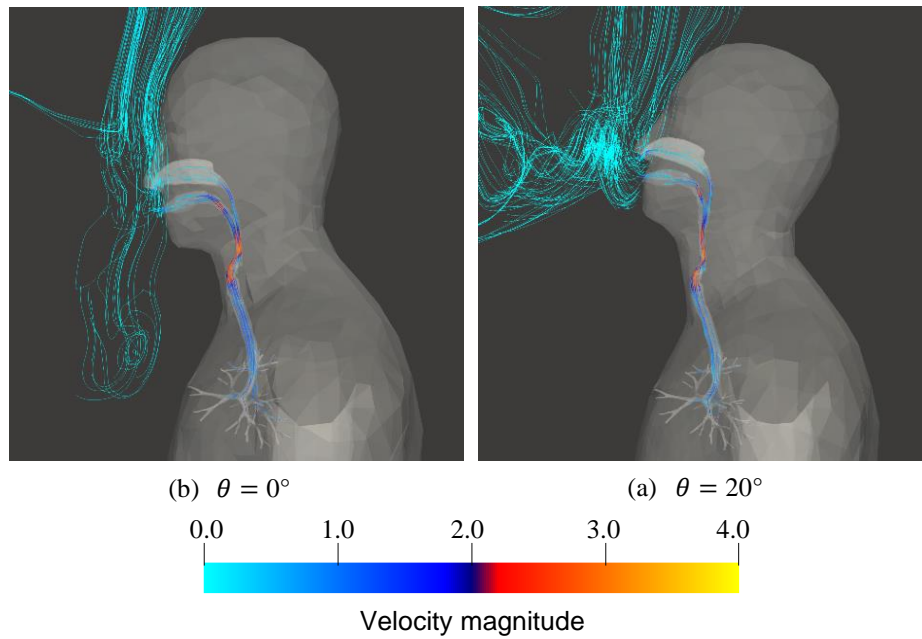


Fig. 11. Streamline of exposed person when the volume flow rate of inhalation took the maximum value ($t = 9.9s$).

5 Conclusions

We comprehensively analyzed the flow field of the room and respiratory regions and evaluated the amount of virus-laden droplet adhered to the inlet patches of the lungs. The angle of an exposed person's neck was also parameterized to simulate the impact of the tilting neck on the risk of infection. In addition, the eighth-generation airway model was used as the airway of an exposed person. It was found that the volume and number of adhered droplets in the right middle region of the bronchi were smaller than other bronchial parts and we confirmed that our finding is consistent with the literature [17]. The total volume and number of adhered droplets increased when the neck angle was 20° upward. This finding suggests that tilting the neck upward facilitates the droplets inhaled into the oral cavity falling into the lungs, i.e., the settling of virus-laden droplets from the oral cavity to lung can be suppressed by facing the head forward instead of tilting the neck upward.

Acknowledgments. This work was supported by JST CREST Grant Number JPMJCR20H7, by JKA through its promotion funds from KEIRIN RACE, and by JSPS KAKENHI Grant Number 21K03856.

References

1. Wang, C.C. et al.: Airborne transmission of respiratory viruses. *Science*, Volume 373, Issue 6558 (2021).
2. Killingley, B. et al.: Safety, tolerability and viral kinetics during SARS-CoV-2 human challenge in young adults. *Nature Medicine* 28, 1031–1041 (2022).
3. Ramajo, D.E., Corzo, S.: Airborne Transmission Risk in Urban Buses: A Computational Fluid Dynamics Study. *Aerosol Air Qual. Res.* 22, 210334 (2022).
4. Mariam. et al.: CFD Simulation of the Airborne Transmission of COVID-19 Vectors Emitted during Respiratory Mechanisms: Revisiting the Concept of Safe Distance. *ACS Omega*, 16876–16889 (2021).
5. Wedel, J. et al.: Anatomy matters: The role of the subject-specific respiratory tract on aerosol deposition - A CFD study, *Computer Methods in Applied Mechanics and Engineering*, Volume 401, Part A, 115372 (2022).
6. Sugiura, N.: Supercomputer finds safest way to sit and chat while eating out. *Asahi Shinbun*, <https://www.asahi.com/ajw/articles/13817552> (2020), last accessed 2023/01/25.
7. Watanabe, N. et al.: An 1D-3D Integrating Numerical Simulation for Engine Cooling Problem. *SAE Technical Paper 2006-01-1603* (2006).
8. Doormal, V.J.P., Raithby, G.D.: Enhancements of the simple method for predicting incompressible fluid flows. *Numerical Heat Transfer*, Vol.7, No.2, 147–163 (1984).
9. van Leer, B.: Towards the Ultimate Conservation Difference Scheme 4: A New Approach to Numerical Convection. *J.Comp. Phys.*, 23, 276–99 (1977).
10. Yoshizawa, A. et al.: *Computational Fluid Dynamics Series 3: Analysis of Turbulent Flows*, University of Tokyo Press, 67–84 (1995).

11. Yamakawa, M. et al.: Computational investigation of prolonged airborne dispersion of novel coronavirus-laden droplets, *Journal of Aerosol Science*, Volume 155, 105769 (2021).
12. Yamakawa, M. et al.: Influenza Viral Infection Simulation in Human Respiratory Tract. In: *The Proceedings of 29th International Symposium on Transport Phenomena*, Paper ID:13, Honolulu Hawaii (2018).
13. Kim, M. et al.: Effect of upper airway on tracheobronchial fluid dynamics. *International Journal for Numerical Methods in Biomedical Engineering*, Volume 34, Issue 9, e3112 (2018).
14. Collier G.J. et al.: 3D Phase Contrast MRI in Models of Human Airways: Validation of Computational Fluid Dynamics Simulations of Steady Inspiratory Flow. *Journal of Magnetic Resonance Imaging*, Volume 48, Issue 5, 1400–1409 (2018).
15. Duguid, J. P. et al.: The size and the duration of air-carriage of respiratory droplets and droplet-nuclei. *Epidemiology & Infection* 44, 6, 471–479 (1946).
16. Bale, R. et al.: Simulation of droplet dispersion in COVID-19 type pandemics on Fugaku. *PASC'21*, Article No.4, 1–11 (2021).
17. Choi, J. et al.: Differences in Particle Deposition Between Members of Imaging-Based Asthma Clusters. *J Aerosol Med Pulm Drug Deliv.* 32(4):213–223 (2019).
18. Atzeni, C. et al.: Computational fluid dynamic models as tools to predict aerosol distribution in tracheobronchial airways. *Sci Rep* 11, 1109 (2021).
19. Gupta, J. K. et al.: Characterizing Exhaled Airflow from Breathing and Talking. *Indoor Air* 20.1 (2010).
20. Fenn, W. O., Rahn, H.: *Handbook of Physiology, Section3: Respiration*, American Physiological Society Washington DC (1965).
21. Ogura, K. et al.: Coupled simulation of Influenza virus between inside and outside the body. In: *The Proceedings of the International Conference on Computational Methods*, Volume 7, 71–82 (2020).